The neurodevelopmental trajectory of beta band oscillations: an OPM-MEG study

Lukas Rier[1+*], Natalie Rhodes[1,2+], Daisie Pakenham[3], Elena Boto[1,4], Niall Holmes[1,4], Ryan M. Hill[1,4], Gonzalo Reina Rivero[1], Vishal Shah[5], Cody Doyle[5], James Osborne[5], Richard Bowtell[1], Margot J. Taylor[2] and Matthew J. Brookes[1,4]

1Sir Peter Mansfield Imaging Centre, School of Physics and Astronomy, University of Nottingham, University Park, Nottingham, NG7 2RD, UK.
2Diagnostic Imaging,The Hospital for Sick Children, 555 University Avenue, Toronto, M5G 1X8, Canada
3Clinical Neurophysiology, Nottingham University Hospitals NHS Trust, Queens Medical Centre, Derby Rd, Lenton, Nottingham NG7 2UH, UK.
4Cerca Magnetics Limited, 7-8 Castlebridge Office Village, Kirtley Drive, Nottingham, NG7 1LD, Nottingham, UK
5QuSpin Inc. 331 South 104th Street, Suite 130, Louisville, Colorado, 80027, USA.

+Indicates authors who made equal contributions to this manuscript.

*Correspondence to:
Dr Lukas Rier,
Sir Peter Mansfield Imaging Centre,
School of Physics and Astronomy,
University of Nottingham,
University Park,
Nottingham NG7 2RD,
United Kingdom
E-mail: lukas.rier@nottingham.ac.uk

Pages: 25
Words: 198 (Abstract), 4709 (Main Body), 1305 (Methods)
Figures: 6
Running title: The neurodevelopmental trajectory of beta band oscillations: an OPM-MEG study

KEYWORDS: Neurodevelopment; beta oscillations; Bursts; Optically pumped magnetometers; Magnetoencephalography

ABSTRACT

Neural oscillations mediate coordination of activity within and between brain networks, supporting cognition and behaviour. How these processes develop throughout childhood is not only a critical neuroscientific question but could also shed light on the mechanisms underlying neurological and psychiatric disorders. However, measuring the neurodevelopmental trajectory of oscillations has been hampered by confounds from instrumentation. In this paper, we investigate the suitability of a disruptive new imaging platform – Optically Pumped Magnetometer-based magnetoencephalography (OPM-MEG) – to study oscillations during brain development. We show how a unique 192-channel OPM-MEG device, which is adaptable to head size and robust to participant movement, can be used to collect high-fidelity electrophysiological data in individuals aged between 2 and 34 years. Data were collected during a somatosensory task, and we measured both stimulus-induced modulation of beta oscillations in sensory cortex, and whole-brain connectivity, showing that both modulate significantly with age. Moreover, we show that pan-spectral bursts of electrophysiological activity drive beta oscillations throughout neurodevelopment, and how their probability of occurrence and spectral content changes with age. Our results offer new insights into the developmental trajectory of oscillations and provide the first clear evidence that OPM-MEG is an ideal platform for studying electrophysiology in children.

INTRODUCTION

Neural oscillations are a fundamental component of brain function. They enable coordination of electrophysiological activity within and between neural assemblies and this underpins cognition and behaviour. Oscillations in the beta range (13-30 Hz) are typically associated with sensorimotor processes [1]; they are prominent over the sensorimotor cortices, diminished in amplitude during sensory stimulation or motor execution, and increased in amplitude (above a baseline level) following stimulus cessation, termed the post-movement beta rebound (PMBR)[2]. Beta oscillations and their modulation by tasks are robustly measured neuroscientific phenomena and their critical importance is highlighted by studies showing abnormalities across a range of disorders – e.g. autism [3], multiple sclerosis [4], Parkinson's disease [5] and Schizophrenia [6]. Despite this, little is known about the mechanistic role of beta oscillations, and most of what is known comes from studies applying non-invasive neuroimaging techniques to adult populations. Whilst the sensorimotor system changes little in adulthood, there are marked changes in childhood and a complete characterisation of the neurodevelopmental trajectory of beta oscillations, particularly how they underpin behavioural milestones, might offer a new understanding of their role in healthy and abnormal brain function.

Several studies have investigated how neural oscillations change with age: Gaetz et al. [7] measured beta modulation during index finger movement, showing that the post-movement beta rebound (PMBR) was diminished in children compared to adults. Kurz et al. [8] reported a similar effect when studying 11-19 year olds executing lower limb movement. Trevarrow et al. [9] found an age related increase in the PMBR amplitude in healthy 9-15 year olds, and further that the decrease in beta power during movement execution did not modulate with age. Finally, Vakhtin et al.[10] showed an increase in PMBR amplitude between adolescence and adulthood, and that this trajectory was abnormal in autism. A separate body of work has assessed neural oscillations in the absence of a task, demonstrating that there is a redistribution of oscillatory power across frequency bands as the brain matures. Specifically, low frequency activity tends to decrease, and high frequency activity increases with age [11–13]. These changes are spatially specific, with increasing beta power most prominent in posterior parietal and occipital regions [14,15]. Beta oscillations are also implicated in long range connectivity [16,17] and previous studies have demonstrated increased connectivity strength with age [18], particularly in attentional networks [19]. In sum, there is accord between studies that show increases in task induced beta modulation and connectivity as well as a redistribution of spectral power, with increasing age.

Despite this progress, neurodevelopmental studies remain hindered by instrumental limitations. Neural oscillations can be measured non-invasively by either magnetoencephalography (MEG) or electroencephalography (EEG). MEG detects magnetic fields generated by neural currents, providing assessment of electrical activity with sub-centimetre spatial, and millisecond temporal precision. However, the sensors traditionally used for field detection operate at low temperature, necessitating the use of fixed 'one-size-fits-all' sensor arrays. Because the signal declines with the square of distance, smaller head size leads to a reduction in signal[20]. In addition, movement relative to fixed sensors degrades data quality. These

limitations mean scanning young children with traditional MEG systems/SQUIDs is challenging. Similarly, there are challenges in EEG. EEG measures differences in electrical potential across the scalp. The electrode array adapts to head shape and moves with the head, making it 'wearable'. However, the resistive properties of the scalp and skull distort signal topography, limiting spatial resolution. EEG is also more susceptible to interference from muscles than MEG [21], particularly during movement. In sum, both EEG and MEG are limited; MEG is confounded by head size, EEG has poor spatial accuracy, and both are degraded by movement. However, in recent years novel magnetic field sensors – Optically Pumped Magnetometers (OPMs) – have inspired a new generation of MEG system [22]. OPMs are small, lightweight and have similar sensitivity to conventional MEG sensors but do not require cryogenics. This enables construction of a wearable MEG system and because sensors can get closer to the head, it provides improved sensitivity and spatial specificity compared to both conventional MEG and EEG [23]. OPM-MEG is, ostensibly, ideal for children; for example, Hill et al. showed the viability of OPM-MEG in a 2 year old [24] and Feys et al. showed advantages for epileptic spike detection in children [25]. However, no studies have yet used OPM-MEG in large groups to measure neurodevelopment.

In addition to instrumental limitations, most neurodevelopmental studies have used an approach to data analysis where signals are averaged over trials. This has led to the idea that sensory induced beta modulation comprises a drop in oscillatory amplitude during movement and a smooth increase on movement cessation. However, recent studies [26–28] investigating unaveraged signals show that, rather than a smooth oscillation, the beta rhythm is, in part, driven by discrete punctate events, known as "bursts". Bursts occur with a characteristic probability, which is altered by a task[29,30], and are not confined to the beta band but are pan-spectral, with components falling across many frequencies [6,30]. There is also evidence that functional connectivity is driven by bursts that are coincident in time across spatially separate regions [30]. Recent work using EEG has found that, even in children as young as 12 months, beta band activity is driven by bursts [31]. These studies have changed the way that the research community thinks about oscillations [32] and a full understanding of beta dynamics and their age dependence must be placed in the context of the burst model.

Here, we combine OPM-MEG with a burst analysis based on a Hidden Markov Model (HMM) [30,33,34] to investigate beta dynamics during a somatosensory task in a large range of young children. Our study addresses two objectives: First, we test the viability of a novel 192-channel triaxial OPM-MEG system for use in paediatric populations, investigating its practicality in young children (from age 2 years) and assessing whether previously observed age-related changes in task-induced beta modulation and functional connectivity can be reliably measured using OPM-MEG. Second, we investigate how task-induced beta modulation in the sensorimotor cortices is related to the occurrence of pan-spectral bursts, and how the characteristics of those bursts change with age.

RESULTS

Our OPM-MEG system comprised a maximum of 64 OPMs (QuSpin Inc., Colorado, USA) each capable of measuring magnetic field independently in three orthogonal orientations, meaning data were recorded using up to 192-channels. Sensors were mounted in 3D-printed helmets of differing size (Cerca Magnetics Ltd. Nottingham, UK), allowing adaptation to the participant's head (Figure 1A). The total weight of the helmet ranged from ~856 g (in the smallest case) to ~906 g (in the largest case). The system was integrated into a magnetically shielded room (MSR) equipped with an active field control system (see "coils" in Figure 1A-B; Cerca Magnetics Ltd. Nottingham, UK) which allowed reduction of background field to <1 nT. This was to ensure that participants were able to move during a scan without compromising sensor operation [35,36]. A schematic of the system is shown in Figure 1B.

27 children (aged 2-13 years) and 26 adults (aged 21-34 years) took part in the study. All participants performed a task in which two stimulators (Figure 1C) delivered somatosensory stimulation to either the index or little finger of the right hand sequentially. Stimuli lasted 0.5 s, occurred every 3.5 s, and comprised three taps on the fingertip. This pattern of stimulation was repeated, alternating 42 times between both fingers. Throughout the experiment, participants could watch their favourite TV show. Following data preprocessing, high fidelity data were available in 27 children and 24 adults Two datasets were excluded from further analysis as data quality was not sufficient to perform our Hidden Markov Model analysis (see Methods). We removed 19 ± 12 % (mean ± standard deviation) of trials in children, and 9 ± 5 % of trials in adults due to excessive interference. On average we had 160 ± 10 channels with high quality data available (note that not all sensors were available for every measurement – see also Discussion).

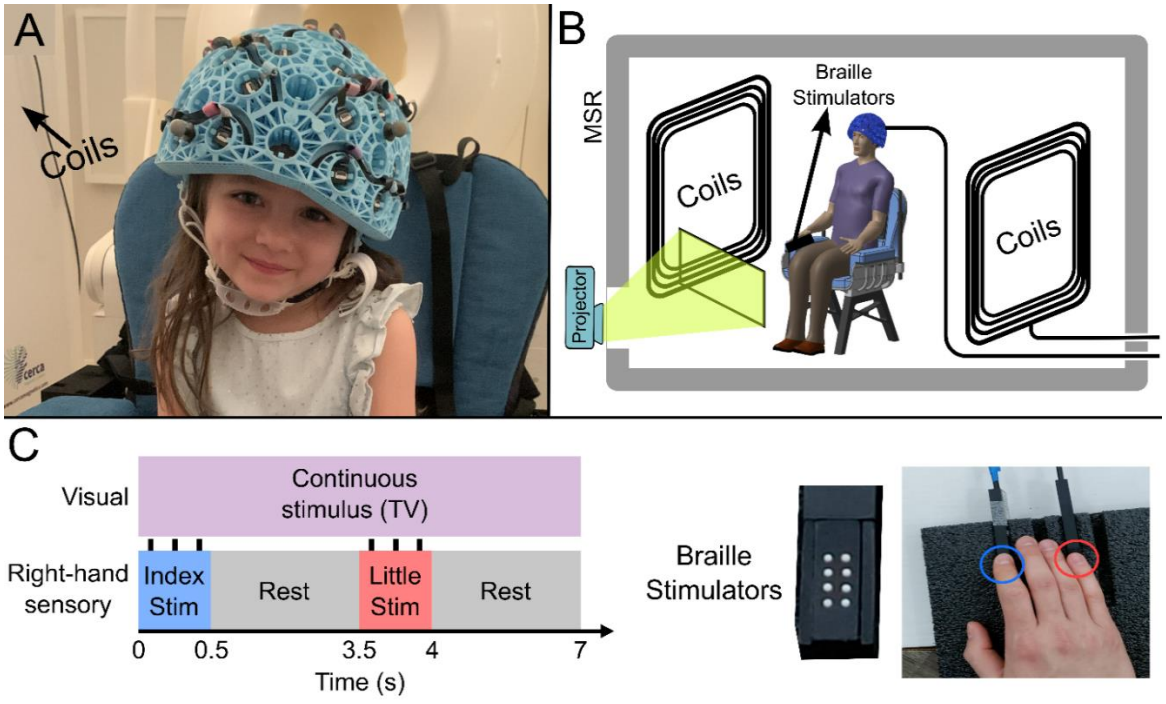

Figure 1 Experimental setup and beta band modulation during sensory task. *(A) 4-year-old child wearing an OPM-MEG helmet. (B) Schematic diagram of the whole system inside the shielded room. (C) Schematic illustration of stimulus timings and a photo of the somatosensory stimulators. "Braille" stimulators each comprise 8 pins, which can be controlled independently; all 8 were used simultaneously to deliver the stimuli.*

Beta band modulation with age

Figure 2 shows beta band modulation during the task for a single representative child (7 years old). Panel A shows the estimated brain anatomy (see Methods) with the locations of the largest beta desynchronisation – contrasted between a stimulus period (0.3-0.8 s relative to stimulus onset) and rest (2.5-3 s) – for index and little finger simulation (derived using a beamformer analysis (see Methods)) overlaid in blue and red respectively. The largest effects fall in the sensorimotor cortices as expected. Panel B shows time frequency spectra depicting the temporal evolution of the amplitude of neural oscillations. Blue represents a decrease in oscillatory amplitude relative to baseline (2.5-3 s); yellow represents an increase. As expected, there is a reduction in beta amplitude during stimulation

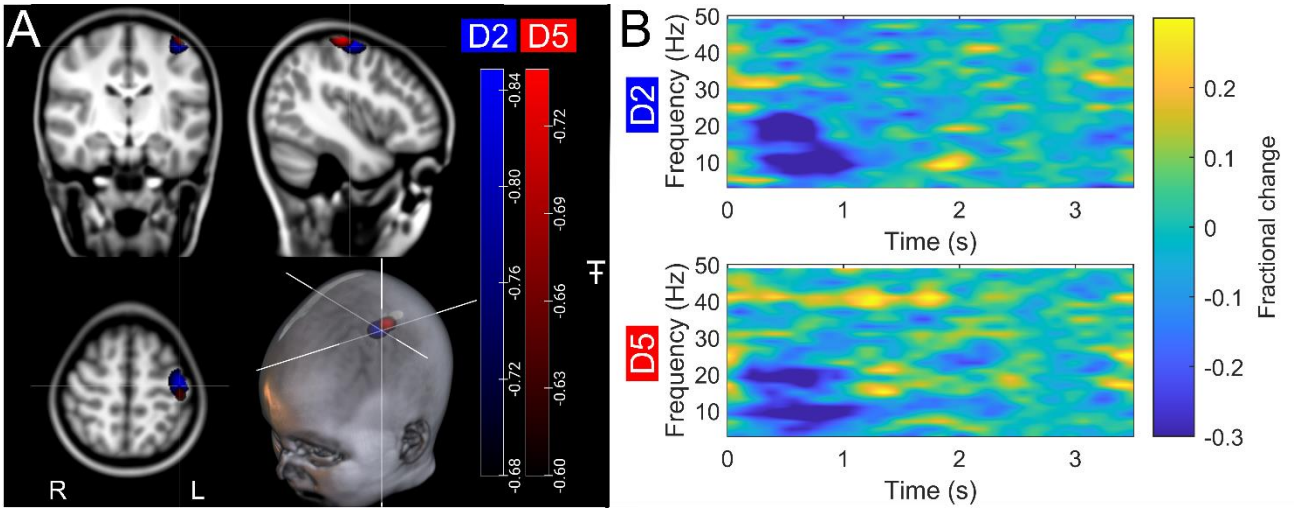

Figure 2: Data from a single participant: *(A) Brain plots show slices through the left motor cortex, with a pseudo-T-statistical map of beta modulation for a single 7-year-old participant. The blue peaks indicate locations of largest beta amplitude reduction during stimulation for index finger trials (digit 2/D2), while the red peaks show the little finger (digit 5/D5). (B) Time frequency spectra showing neural oscillatory amplitude modulation (fractional change in spectral amplitude relative to baseline measured in the 2.5-3 s window) for both fingers, using data extracted from the location of peak beta modulation (left sensorimotor cortex). Note the beta amplitude reduction during stimulation, as expected.*

Group averaged beta dynamics are shown in Figure 3. Here, for visualisation, the children were split into three groups of 9: youngest (aged 2 – 6 years), middle (6 to 10 years), and oldest (10 to 13 years). Data were averaged within each group, and across all 24 adults (21 – 34 years) for comparison. The brain plots show group averaged pseudo-T statistical maps of stimulus induced beta band modulation. In all groups, the peak modulation appeared in the left sensorimotor cortex. We observed no significant difference in the location of peak beta desynchronisation between index and little finger stimulation (see also Discussion). The time-frequency spectrograms (TFSs) are also shown for each group. Here, we observe a drop in beta amplitude during stimulation for all 3 groups, however this was most pronounced in adults and was weaker in younger children. For statistical analysis, we estimated the difference in beta-band amplitude between the stimulation (0.3-0.8 s) and post-stimulation (1-1.5 s) windows and plotted this as a function of age (Figure 3B) with Pearson correlation suggesting a significant ($R^2 = 0.29, p = 4 \times 10^{-5}$) relationship. These data

agree strongly with previous studies showing increased task induced beta modulation with age. However, they are acquired using a fundamentally new wearable technology, and in younger participants.

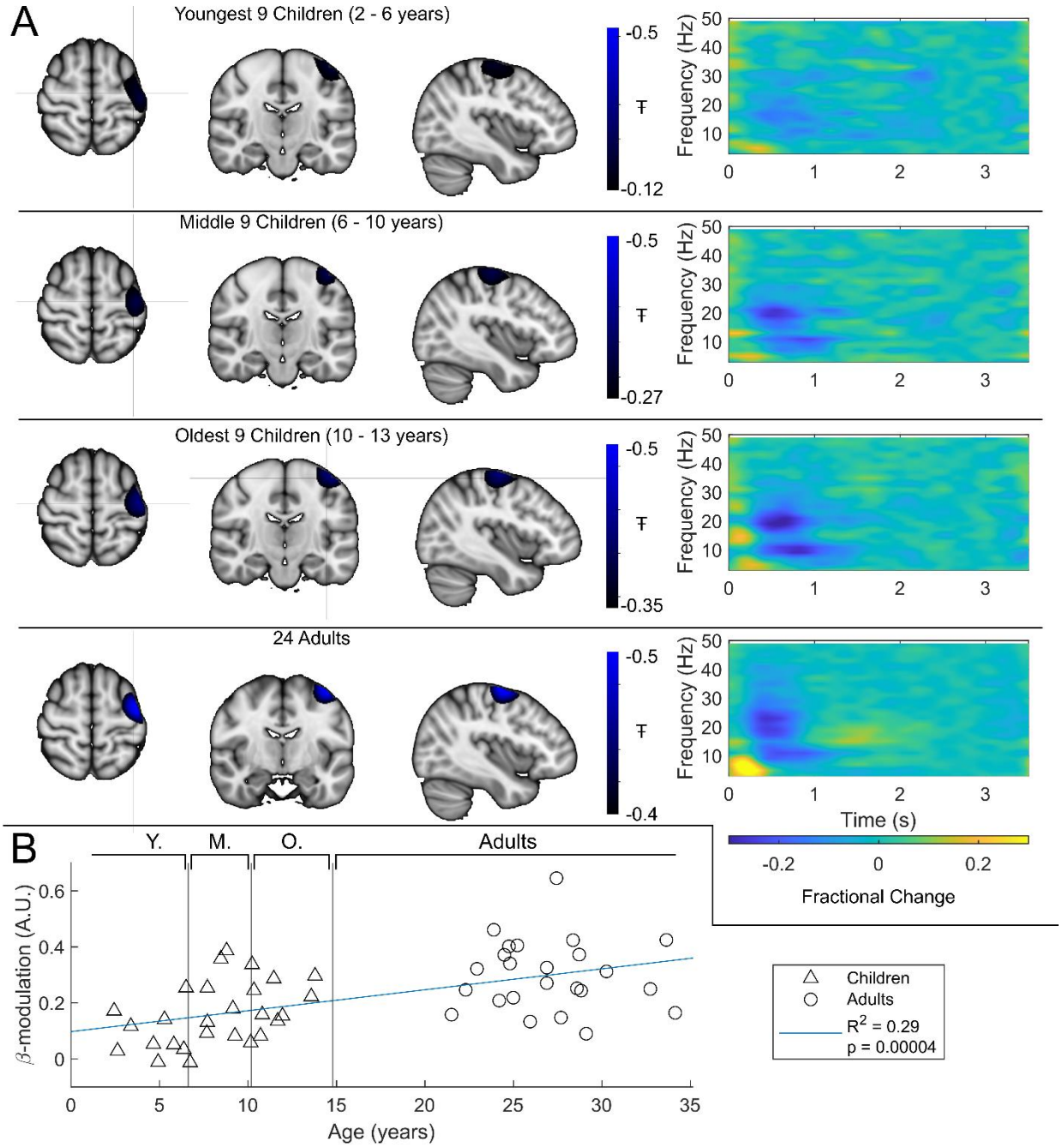

Figure 3: Beta band modulation with age: *(A) Brain plots show slices through the left motor cortex, with a pseudo-T-statistical map of beta modulation (blue/black) overlaid on the standard brain. Time frequency spectrograms show modulation of the amplitude of neural oscillations (fractional change in spectral amplitude relative to the baseline measured in the 2.5-3 s window). In all cases results were extracted from the location of peak beta desynchronisation (in the left sensorimotor cortex). Note the clear beta amplitude reduction during stimulation. (B) Difference in beta-band amplitude (0.3-0.8 s window vs 1-1.5 s window) plotted as a function of age (i.e., each data point shows a different participant; triangles represent children, circles represent adults). Note significant correlation (*$R^2=0.29, p=0.00004$**). Also, all data here relate to the index finger stimulation; similar results are available for the little finger stimulation in supplementary information Figure S1.*

Functional connectivity in the beta band:

Whole brain beta-band functional connectivity was estimated by calculating amplitude envelope correlation (AEC)[37] between (unaveraged) beta-band signals extracted from 78 cortical regions. Figure 4A shows connectome matrices averaged across participants in each of the four groups; each matrix element represents the strength of a connection between two brain regions. In the "glass brains", the red lines show the 150 connections with the highest connectivity. In adults, the connectome is in strong agreement with those from previous studies[18,38], with prominent sensorimotor, posterior-parietal- and fronto-parietal connections. However, connectivity patterns in children differed in both strength and spatial signature, with the visual network showing the strongest connectivity. To statistically test the relationship between connectivity and age, we plotted global connectivity (i.e., the sum of all matrix elements) versus age (Figure 4B). Pearson correlation suggested a significant ($R^2 = 0.42, p = 2.67 \times 10^{-7}$) relationship with older participants having increased connectivity. We also probed how this relationship changes across brain regions: Figure 4D shows example scatter plots of node degree (i.e., how connected a specific region is to the rest of the brain) for two pairs of homologous frontal and occipital regions. Note that the gradient of the fit in the frontal regions ($0.27\ age^{-1}$, $R^2 = 0.44, p = 1.2 \times 10^{-7}$ and $0.27\ age^{-1}$, $R^2 = 0.50, p = 5.8 \times 10^{-9}$) is much larger than that in the occipital regions ($0.10\ age^{-1}$, $R^2 = 0.18, p = 2.0 \times 10^{-3}$, $0.12\ age^{-1}$, $R^2 = 0.29, p = 4.2 \times 10^{-5}$.). This is delineated for all brain regions in Figure 4C, where each region is coloured according to the gradient of the fit. The regions showing the largest change with age are frontal and parietal areas, with visual cortex demonstrating the smallest effect.

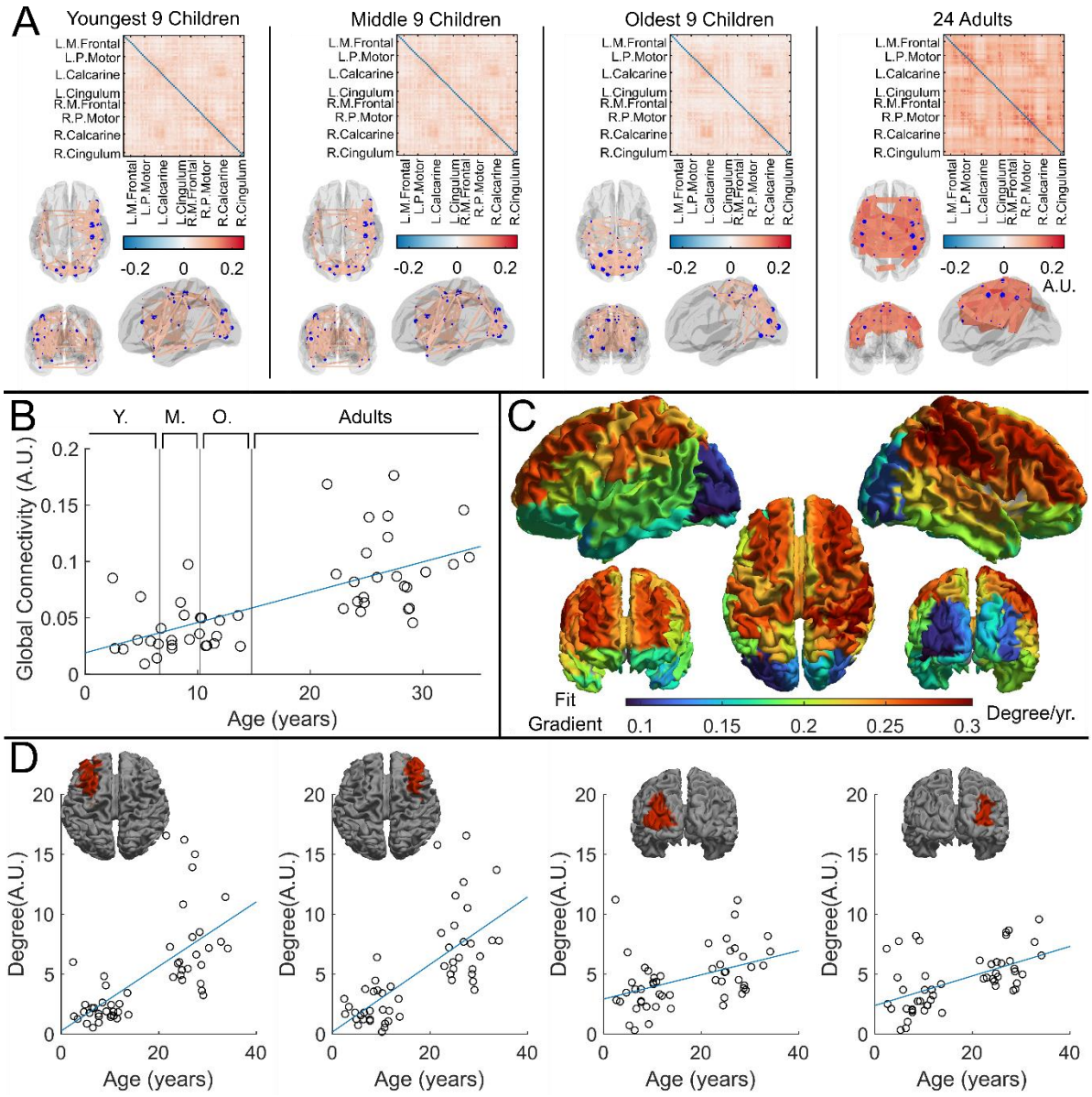

Figure 4 Functional connectivity – estimated using Amplitude Envelope Correlation (AEC) – varies with age. *(A) Connectivity matrices constructed using 78 regions of the AAL atlas and glass brains showing average connectomes across groups and corresponding glass brains showing the strongest 150 connections. AEC was estimated across the entire task recording. (B) Global average connectivity increases significantly with age* ($R^2 = 0.42, p = 2.67 \times 10^{-7}$**). (C) Age-related changes in connectivity vary spatially. Brain plot shows the linear fit gradient of node degree (the sum across the rows of the connectivity matrices) against age. Node degree varies less in occipital regions while frontal regions become more strongly connected with increasing age. (D) Example plots show node degree against age for left and right frontal and occipital regions. Pearson correlation yielded (from left to right):* ($R^2 = 0.44, p = 1.2 \times 10^{-7}, Degree = 0.27 \cdot age + 0.26$)*;* ($R^2 = 0.50, p = 5.8 \times 10^{-9}, Degree = 0.28 \cdot age + 0.17$)*;* ($R^2 = 0.18, p = 2.0 \times 10^{-3}, Degree = 0.10 \cdot age + 2.92$)*;* ($R^2 = 0.29, p = 4.2 \times 10^{-5}, Degree = 0.12 \cdot age + 2.38$)*.*

Burst interpretation of beta dynamics:

To assess pan-spectral bursts, we applied a univariate, 3-state HMM to the broadband (1-48 Hz) electrophysiological signal extracted from the location of largest beta modulation. This enabled us to identify the times at which bursts occurred in sensorimotor cortex [30,39].

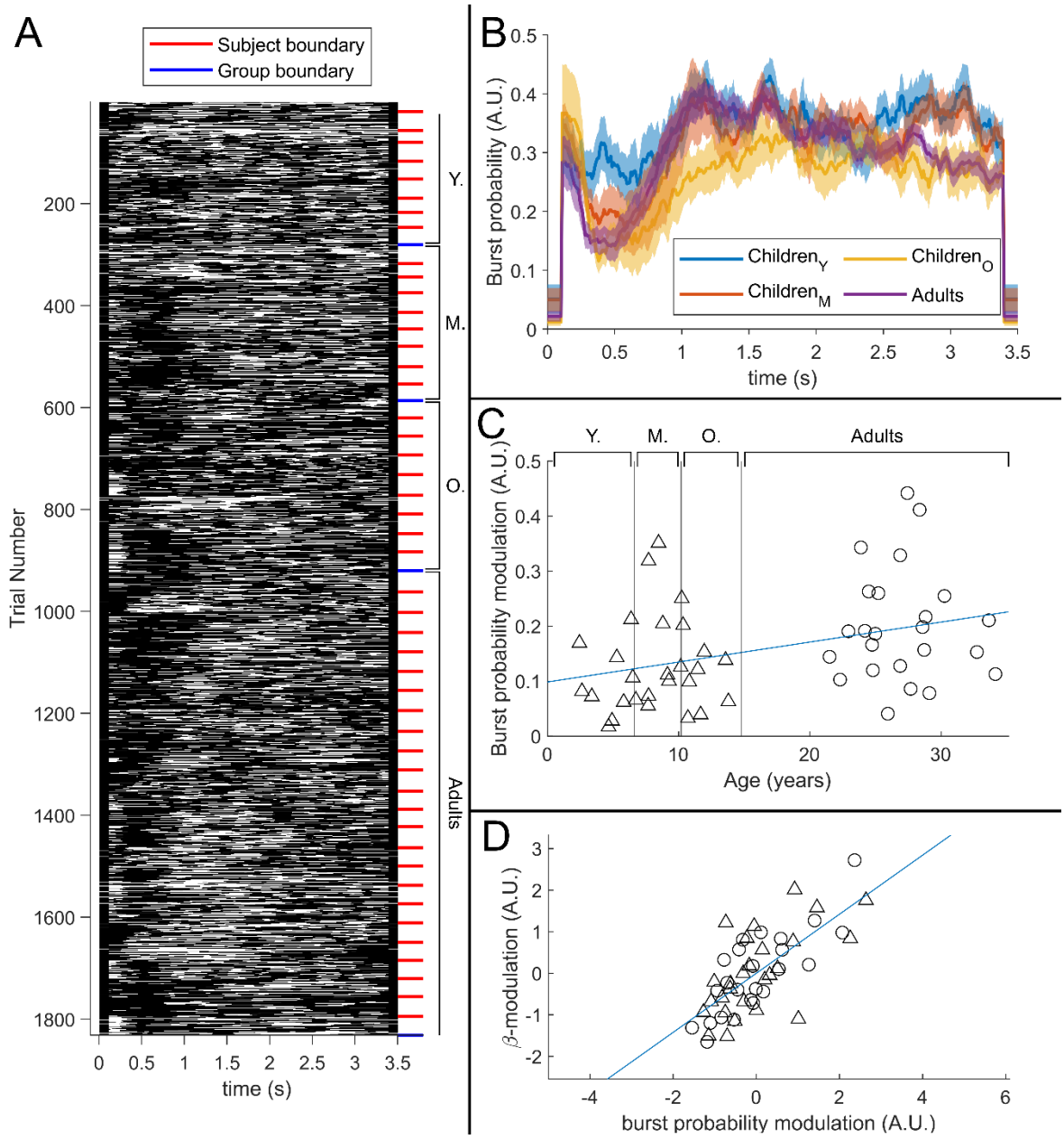

Figure 5: The relationship between beta-band amplitude modulation and pan-spectral burst probability. *(A) Raster plot showing burst occurrence (white) as a function of time for all trials and participants combined (participants sorted by increasing age). (B) Trial averaged burst probability time-courses across the four participant groups. Shaded areas indicate the standard error within groups. (C) Stimulus- to post-stimulus modulation of burst probability (0.3-0.8 s vs 1-1.5 s) plotted against age. Note significant* (R^2=0.13, p=0.0089*) positive correlation. (D) Beta amplitude modulation plotted against burst probability. Note again significant correlation* ($R^2 = 0.5, p = 5.2 \times 10^{-9}$*). (Values for both measures were z-transformed within the Children and Adult group respectively to mitigate the age confound). Triangles and circles denote Children and Adults respectively.*

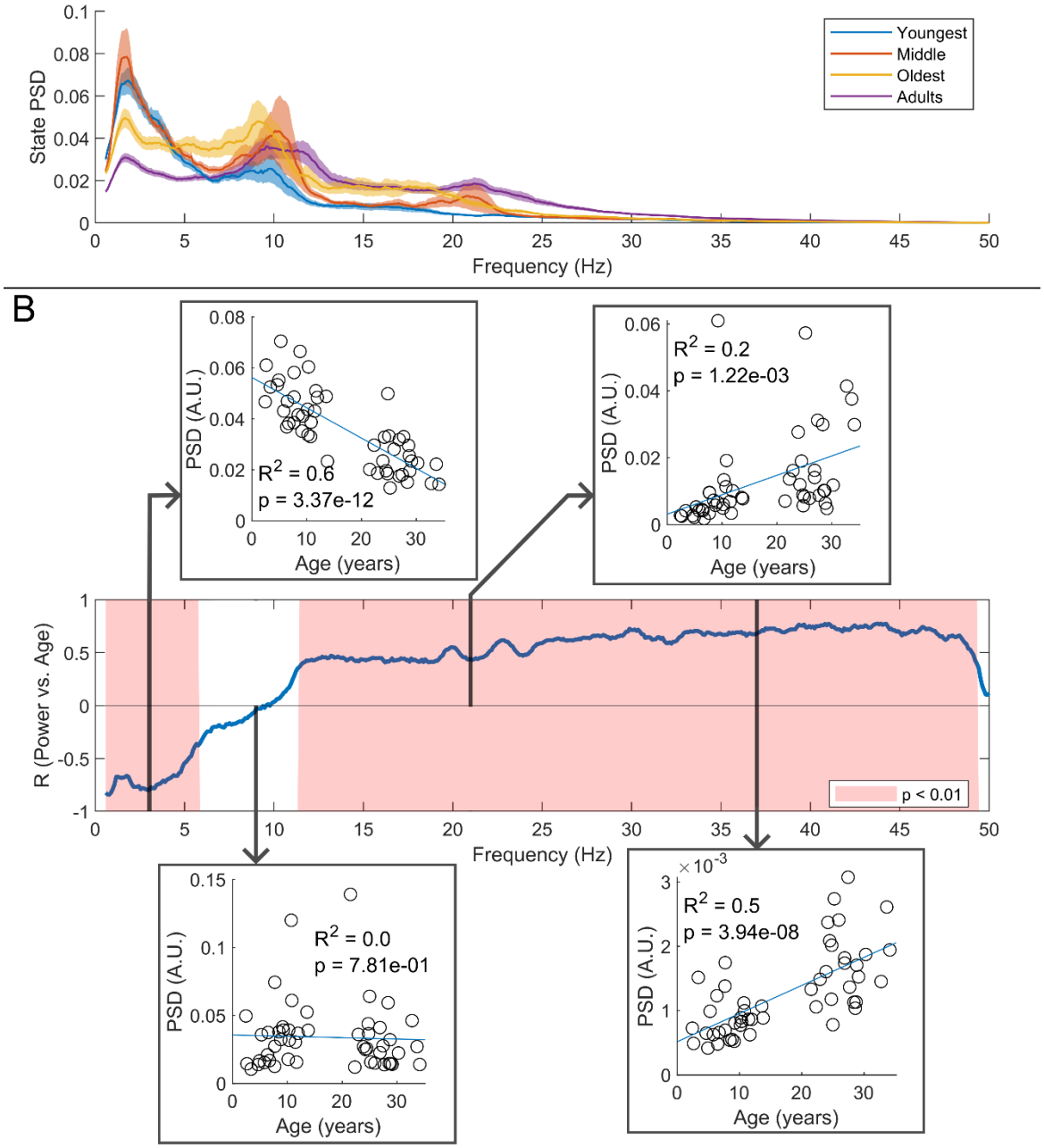

Figure 6: Spectral content of the burst state varies with age. *(A) Average burst-state spectra across groups. Shaded areas indicate standard error on the group mean. (B) Pearson correlation coefficient for the PSD values in (A) against age across all frequency values. Red shaded areas indicate* $p < 0.01$ *(uncorrected). The four inset plots show example scatters of PSD values with age at select frequencies (3 Hz, 9 Hz, 21 Hz, and 37 Hz). Low-frequency spectral content decreases with age while high-frequency content increases. No significant correlation was observed in the high theta and alpha bands.*

Figure 5A shows a raster plot of burst occurrence for all individual task trials in all participants. White represents time points and trials where bursts are occurring; black represents the absence of a burst. Participants are separated by the red lines and groups are separated by the blue lines. Burst absence is more likely in the 0.3 s to 0.8 s time-period (during stimulation), indicating a task-induced decrease in burst-probability. Figure 5B shows group averaged burst-probability as a function of time. In all age groups, bursts were less likely during stimulation, though this modulation changes with age, with the younger group demonstrating the least pronounced effect. This is tested statistically in Figure 5C which shows a significant

($R^2 = 0.13, p = 8.9 \times 10^{-3}$*) positive Pearson correlation between the modulation of burst probability and age. Figure 5D shows the association between beta amplitude and burst-probability modulation. Here the significant ($R^2 = 0.50, p = 5.2 \times 10^{-9}$*) positive relationship supports a hypothesis that the observed change in task induced beta modulation with age (shown in Figure 3) is driven by changes in the modulation of burst probability.

We estimated the spectral content of the bursts identified by the HMM. In Figure 6A the burst spectra are shown for all 4 participant groups. In adults, the spectral power diminishes with increasing frequency, with additional peaks in the alpha and beta band. In children, high frequencies are diminished, and low frequencies are enhanced, compared to adults. This is also shown in Figure 6B where, for every frequency, we perform a linear fit to a scatter plot of spectral density versus age. Here, positive values indicate that spectral power increases with age; negative power means it decreases. The inset scatter plots show example age relationships at 3 Hz, 9 Hz, 21 Hz, and 37 Hz. We see a clear decrease in low-frequency spectral content and increasing high-frequency content, with age. Interestingly, spectral content in the alpha band appeared stable with no significant correlation with age. Similar trends for changes in frequency content with age were found for the non-burst states (See Figure S2).

DISCUSSION

There are few practical, non-invasive neuroimaging platforms capable of measuring brain function in children with good spatial and temporal resolution. Functional magnetic resonance imaging (fMRI) [40] tracks brain activity with millimetre spatial resolution, but the mechanism of detection is indirect (based on haemodynamic responses) and consequently fMRI has limited temporal precision. Participants must also lie immobile in a large scanner while being exposed to high acoustic noise; many children find this environment challenging and it is difficult to implement naturalistic experimental paradigms. Functional near infra-red spectroscopy (fNIRS) [41] also measures haemodynamics, but provides a wearable platform which allows scanning of almost any participant during any conceivable experiment. However, fNIRS has limited temporal resolution since measurements are driven by changes in blood flow and metabolism. fNIRS also has limited (~1 cm) spatial resolution and is only sensitive to superficial sources. EEG [42] measures electrophysiological activity in neural networks and thus offers millisecond temporal precision. In addition, EEG is wearable, adaptable to any participant, and therefore enables naturalistic experiments. However, spatial resolution is restricted due to the inhomogeneous conductivity profile of the head (a problem made more challenging in very young (<18 months) children due to additional inhomogeneities caused by the fontanelle). EEG is also highly susceptible to artefacts from electrical activity in muscles. Conventional MEG [43] offers both excellent spatial and temporal resolution for non-invasive measurement of brain electrophysiology but is nevertheless limited in both performance and practicality – particularly in young people – due to the fixed nature of the sensor array. It therefore follows that the technologies currently in use for neurodevelopmental assessment are limited by either practicality, performance, or both. Development of new techniques for use in this area

is therefore of high importance. In principle, OPM-MEG offers the performance of MEG, with the practicality of fNIRS or EEG, making it extremely attractive for use in children. Here, our first aim was to test the feasibility of this platform for neurodevelopmental studies.

We designed our OPM-MEG system for lifespan compliance. The helmets were relatively lightweight, ranging from ~856 g (in the smallest case) to ~906 g (in the largest case). While this is heavier than, for example, a child's bicycle helmet (the average weight of which is ~300-350 g) they were well tolerated by our cohort, most likely due to the relatively short scanning duration of < 5 minutes. Multiple sizes of helmet meant we could select the best fitting size for any given participant, reducing the confounds of small head size which are associated with conventional MEG. Heat from the sensors (which require elevated temperature to maintain operation in the spin exchange relaxation free regime [44]) was controlled via both convection cooling, with air being able to flow through the helmet lattice, and an insulating material cap worn under the helmet by all participants (See Figure 1A). Together, these ensured that participants remained comfortable throughout data recording.

Whilst the helmet allows sensors to move with the head, the sensors are perturbed by background fields (e.g., if a sensor rotates in a uniform background field, or translates in a field gradient, it will see a changing field which can obfuscate brain activity and, in some cases, stop the sensors working [23]). For this reason, our system also employed active field control [36] which enabled us to reduce the field to a level where sensors work reliably, even in the presence of head movements. This meant that, although we did not encourage our participants to move, they were completely unrestrained. The sensors themselves are robust to head motion: every sensor is a self-contained unit connected to its own control electronics by a cable that can accommodate rapid and uncontrolled movement. Another challenge when imaging children is the proximity of the brain to the scalp – the brain-scalp separation is 15 mm in adults but can be as little as 5 mm in children. Previous work [45] has shown that, when using radially oriented field measurements, a combination of finite sampling and the proximity of the brain can lead to inhomogeneous coverage (i.e. spatial aliasing). For this reason, our system was designed with triaxial sensors which helps to prevent this confound (though not directly related to scanning children, we also note that triaxial sensors enable improved noise rejection [46,47]). Finally, our system was housed in a large MSR which allowed children to be accompanied by a parent throughout the scan. All these design features led to a system that enables acquisition of high-quality MEG data and is also well tolerated. We were able to obtain usable data in 27 out of 27 children and 24 out of 26 adults. Our findings of increased beta modulation and whole brain connectivity with age support previous studies[7–9,18], and in this way provide a validation for this technology.

Importantly, most prior studies of neurodevelopmental trajectory were carried out in older children – for example Kurz et al. [8] showed a similar effect in 11-19 year olds; Trevarrow et al. [9] employed a cohort of 9-15 year olds and our own previous work also scanned a cohort of 9-15 year olds [19]. In the present study, we were able to successfully scan children from age 2 years. There are important reasons for moving to younger participants: from a neuroscientific viewpoint, many critical milestones in development occur in the

first few years (even months) of life – such as learning to walk and talk. If we can use OPM-MEG technology to measure the brain activities that underpin these developmental milestones, this would offer not only a new understanding of brain function but also new avenues to explore in atypically developing children. More importantly, many disorders strike in the first years of life – for example autism can be diagnosed in children as young as two years and epilepsy has a high incidence in children, including in the neonatal and infant period [48]. In those where seizures cannot be controlled by drugs, surgery is often a viable option for treatment; the younger the patient, the more successful the outcome[49]. For these reasons, the development of a platform that enables the assessment of brain electrophysiology, with high spatiotemporal precision, in young people is a significant step forward and one that has potential to impact multiple neuroscientific and clinical areas.

In addition to providing a new platform for neurodevelopmental investigation, our study also provides insights into coordinated brain activity and its maturation with age. Beta band oscillations are thought to mediate top-down influence on primary cortices, with regions of high beta amplitude likely being inhibited (for a review see Barone and Rossiter [1]). Whilst most evidence is based on studies of movement, there is significant supporting evidence from somatosensory studies in adults; for example Bauer et al. [50] showed that, when one attends to events relating to the left hand, a relative decrease in beta amplitude is seen in the contralateral sensory cortex (right) and an increase in ipsilateral cortex – suggesting the brain is inhibiting the sensory representation of the non-relevant hand. Given this strong link to attentional mechanisms and top-down processing, it is unsurprising that beta oscillations are not fully developed in children, and consequently change with age. Interestingly, Figure 3 implies that the well-known post stimulus beta signal – the PMBR – appears to be absent in children but can be seen in adults. The rebound, as well as being linked to top-down inhibition of the sensorimotor cortex, is associated with long range connectivity [51]. The lack of rebound is therefore in agreement with the connectivity findings shown in Figure 4. We failed to see a significant difference in the spatial location of the cortical representations of the index and little finger; there are three potential reasons for this. First, the system was not designed to look for such a difference – sensors were sparsely distributed to achieve whole head coverage (rather than packed over sensory cortex to achieve the best spatial resolution in one area). Second, our "pseudo-MRI" approach to head modelling is less accurate than acquisition of participant-specific MRIs, and so may mask subtle spatial differences. Finally, previous work [52] suggested that, for a motor paradigm in adults, only the beta rebound, and not the power reduction during stimulation, mapped motortopically. Nevertheless, it remains the case that by placing sensors closer to the scalp, OPM-MEG should offer improved spatial resolution in children and adults; this should be the topic of future work.

The burst model of beta dynamics is relatively new, yet significant evidence already shows that the neurophysiological signal is driven by punctate bursts of activity, whose probability of occurrence changes depending on the task phase. Our study provides the first evidence that neurodevelopmental changes in the amplitude of task induced beta modulation can also be explained by the burst model. Specifically, we showed

that task induced modulation of burst probability changes significantly as a function of age, suggesting bursts in somatosensory cortex are less likely to occur during stimulation of older participants compared to younger participants. We also showed that the "classical" beta band modulation exhibited a significant linear relationship with burst-probability modulation. In addition, when bursts do occur, they tend to have different spectral properties in younger participants. Specifically, younger participants have increased low-frequency activity and decreased high frequency activity, compared to adults. It is likely that a combination of the change in burst probability with age, and the change in dominant frequency (away from the canonical beta band) drives the observation from previous studies of changing beta modulation with age.

Our connectivity finding is also of note, showing a significant increase in functional connectivity with age. This is in good agreement with previous literature – for example Schäfer et al. [18] showed quantitatively similar data in conventional MEG, albeit again by scanning older children (ages 6 and up). Here we also showed that connectivity changes with age are most prominent in the frontal and parietal areas, and weakest in the visual cortex. It makes intuitive sense that the largest changes in connectivity over the age range studied should occur in the parietal and frontal regions – these regions are typically associated with both cognitive and attentional networks and are implicated in the networks that develop most between childhood and adulthood. Here, we observed a relative lack of age-related change in the visual regions; this could relate to the nature of the task – recall that all volunteers watched their favourite TV show and so the visual regions were being stimulated throughout, driving coordinated network activity in occipital cortex. The visual system is also early to mature compared to frontal cortex.

There are four limitations of our system which warrant discussion. Firstly, the range of available helmets was limited, and future studies may aim to use more sizes to better accommodate variation in head size and shape. Also, even the lightweight helmet used here may be too heavy for younger participants; whilst in general it was tolerated very well, anecdotally, some of the very young participants commented that it was heavy. This indicates that further optimisation of helmet-weight is needed if we want to move towards younger (< 2 years) participants; in babies a fundamentally different solution must be found. Further optimisation is possible since, whilst the total weight is approximately 900 g, the combined sensor weight is just 250g. Similarly, the warmth generated by the sensors was controlled by a combination of convection and insulation. However, for systems with a higher channel count, where more heat may be generated, active cooling (e.g., air forced through the helmet) may be required. Second, the number of sensors available varied across participants – this was mainly for pragmatic purposes (the system was experimental and not all OPMs were available for every recording). Whilst we always ensured good coverage of sensorimotor cortex, and tried to optimise whole brain coverage as much as we could, the system is likely to have diminished sensitivity around the temporal cortex, and this may explain why there was relatively little change in connectivity with age in those regions. In future, the inclusion of more sensors, particularly around the cheekbone would be a natural extension. Thirdly, magnetic field control was only available over a region encompassing the head, whilst participants were seated (i.e., participants had to be sat in a chair for the scanner to work). This was

key to ensuring participants were unconstrained. However, in future studies, particularly in younger participants, it may be desirable to accommodate different positions (e.g., participants seated on the floor) and a greater range of motion (e.g., children crawling or walking). This may be possible with newly developing coil technology [53]. Finally, here we chose to study sensory stimulation. There are many other systems to choose – and whether the findings here regarding beta bursts and the changes with age also extend to other brain networks remains an open question that could be explored in future studies.

CONCLUSION

Characterising how neural oscillations change with age is a key step towards understanding the developmental trajectory of coordinated brain function, and the deviation of that trajectory in disorders. However, limitations of conventional, non-invasive approaches to measuring electrophysiology have led to confounds when scanning children. Here, we have demonstrated a new platform for neurodevelopmental assessment. Using OPM-MEG, we have been able to provide evidence – supported by previous studies – that shows both task-induced beta modulation and whole brain functional connectivity increase with age. In addition, we have shown that the classically observed beta power drop during stimulation can be explained by a lower burst probability, and that modulation of burst probability changes with age. We further showed that the frequency content of bursts changes with age. Our results offer new insights into the developmental trajectory of beta oscillations and provide the first clear evidence that OPM-MEG is an ideal platform to study electrophysiology in children.

METHODS

Participants and Experiment

The paradigm comprised tactile stimulation of the tips of the index and little fingers using two braille stimulators (METEC, Germany) (See Figure 1C). Each stimulator comprised 8 independently controlled pins which could be raised or lowered to tap the participant's finger. A single trial comprised 0.5 s of stimulation (during which the finger was tapped 3 times using all 8 pins) followed by 3 s rest and the finger stimulated (index or little) was alternated between trials. There was a total of 42 trials for each finger, meaning the experiment lasted a total of 294 s. Throughout the experiment, participants watched a television program of their choice (presented via projection onto a screen in the MSR). All children were accompanied inside the MSR by a parent and one experimenter throughout their visit.

Data collection and co-registration

The sensor array comprised 64 triaxial OPMs (QuSpin Inc, Colorado, USA, Zero Field Magnetometer, Third Generation, Triaxial Variant) which enabled a maximum of 192 measurements of magnetic field around the scalp (192-channels). The OPMs could be mounted in one of four 3D-printed helmets of different sizes (Cerca Magnetics Ltd., Nottingham, UK); this affords (approximate) whole-head coverage and adaptation to the participants head size. All participants wore a thin aerogel cap underneath the helmet to control heat

from the sensors (which operate with elevated temperature). The system is housed in a magnetically shielded room (MSR) equipped with degaussing coils [54] and active magnetic field control [36] (Cerca Magnetics Ltd., Nottingham, UK). Prior to data collection, the MSR was demagnetised and the magnetic field compensation coils were enabled (using currents based on previously obtained field maps, the demagnetisation procedure ensures a repeatable background field and the magnetically quiet campus location of our MSR ensures field drifts <0.05 nT/min [55,56]). This procedure, which results in a background field of ~0.6 nT [56], is important to enable free head motion during a scan [57]. All OPMs were equipped with on-board coils which were used for sensor calibration. MEG data were collected at a sampling rate of 1,200 Hz using a National Instruments (NI, Texas, USA) data acquisition system interfaced with LabVIEW (NI).

Following data collection, two 3D digitisations of the participant's head, with and without the OPM helmet, were generated using a 3D structured light metrology scanner (Einscan H, SHINING 3D, Hangzhou, China). Participants wore a swimming cap to flatten hair during the 'head-only' scan. The head-only digitisation was used to measure head size and shape, and an age-matched T1-weighted template MRI scan was selected from a database [58] and warped to fit the digitisation, using FLIRT in FSL [59,60]. This procedure resulted in a "pseudo-MRI" which provided an approximation of the subject's brain anatomy. Sensor locations and orientations relative to this anatomy were found by aligning it to the digitisation of the participant wearing the sensor helmet, and adding the known geometry of the sensor locations and orientations within the helmet [61–63]. This was done using MeshLab [64].

MEG Data Preprocessing

We used a preprocessing pipeline described previously [63]. Briefly, broken or excessively noisy channels were identified by manual visual inspection of channel power spectra; any channels that were either excessively noisy, or had zero amplitude, were removed. Bad trials were defined as those with variance greater than 3 standard deviations from the mean trial variance, and automatically removed. A visual inspection was also carried out and any remaining trials with excess artefacts were removed. Notch filters at the powerline frequency (50 Hz) and 2 harmonics, and a 1-150 Hz band pass filter, were applied. Finally, eye blink and cardiac artefacts were removed using ICA (implemented in FieldTrip [65]) and homogeneous field correction (HFC) was applied to reduce interference [66].

Source Reconstruction and Beta-Modulation

For source estimation, we used a LCMV beamformer spatial filter [67]. For all analyses, covariance matrices were generated using data acquired throughout the whole experiment (excluding bad channels and trials). Covariance matrices were regularised using the Tikhonov method with a regularisation parameter equal to 5% of the maximum eigenvalue of the unregularized matrix. The forward model was based on a single shell volumetric conductor [68].

To construct the **Pseudo-T statistical images**, data were filtered to the beta-band (13-30 Hz) and narrow band data covariance matrixes generated. Voxels were placed on both an isotropic 4-mm grid

covering the whole brain, and a 1-mm grid covering the contralateral sensorimotor regions. For each voxel, we contrasted power in active (0.3-0.8 s) and control (2.5-3 s) time windows to generate images showing the spatial signature of beta band modulation. Separate images were derived for index and little finger trials. To generate **time frequency spectra,** we used broad-band (1-150 Hz) data and covariance matrices. The beamformer was used to produce a time course of neural activity (termed a "virtual electrode") at the voxel with maximum beta-band desynchronisation. The resulting projected broad-band data were frequency filtered into a set of overlapping bands, and a Hilbert transform used to derive the analytic signal for each band. The absolute value of this was computed to give the envelope of oscillatory amplitude (termed the Hilbert envelope). This was averaged across trials, concatenated in frequency, baseline corrected and normalised yielding a time frequency spectrogram showing relative change in spectral power (from baseline) as a function of time and frequency. Finally, to quantify the magnitude of **beta-modulation**, we filtered the virtual electrode to the beta band, calculated the Hilbert envelope and measured the mean difference in amplitude between stimulation (0.3-0.8 s) and post-stimulus (1-1.5 s) time windows. These values (derived for every participant) were plotted against age and a relationship assessed via Pearson correlation.

Functional Connectivity Analysis

To estimate connectivity, we first parcellated the brain into distinct regions. To this end, estimated brain anatomies were co-registered to the MNI standard brain using FSL FLIRT [59,60] and divided into 78 cortical regions according to the Automated Anatomical Labelling (AAL) atlas [69–71]. Virtual electrode timecourses were generated at the centre of mass of each of these 78 regions, and the beta band Hilbert envelope derived. We then computed Amplitude Envelope Correlation (AEC) as an estimate of functional connectivity between all possible pairs of AAL regions [17,37]. Prior to AEC, we applied pairwise orthogonalisation to reduce source leakage [72,73]. This resulted in a single connectome matrix per participant. We estimated "Global Connectivity" as the mean connectivity value across all elements in the connectome. This was plotted against age and the relationship assessed using Pearson correlation. To visualise the spatial variation in age-related connectivity changes, we also estimated the correlation between node degree (i.e., the column-wise sum of connectome matrix elements) and age, for each of the 78 AAL regions.

Beta Bursts and Hidden Markov Modelling

To estimate beta burst timings we employed a three-state, time-delay embedded univariate HMM[34]. This method has been described extensively in previously papers [30,39]. Briefly, virtual electrode time series were frequency filtered between 1-48 Hz. The HMM was used to divide this timecourse into three "states" each depicting repeating patterns of activity with similar temporo-spectral signatures. The output was three timecourses representing the likelihood of each state being active as a function of time. These were binarized (using a threshold of 2/3) and used to generate measures of the probability of state occurrence as a function of time in a single trial. The state whose probability of occurrence modulated most with the task was defined as the "burst state". We estimated age-related changes in burst probability modulation and the relationship

between burst probability modulation and classical beta-modulation (see above) using Pearson correlation. Further, we investigated the spectral content of the burst state and its modulation with age using multi-taper estimation of the power spectral density (PSD) [34]. Having derived the spectral content of the burst state we used Pearson correlation to measure how the PSD magnitude, for every frequency, changes with age.

ACKNOWLEDGEMENTS

This work was supported by an Engineering and Physical Sciences Research Council (EPSRC) Healthcare Impact Partnership Grant (EP/V047264/1) and an Innovate UK germinator award (Grant number 1003346). We also acknowledge support from the UK Quantum Technology Hub in Sensing and Timing, funded by EPSRC (EP/T001046/1), a Wellcome Collaborative Award in Science (203257/Z/16/Z and 203257/B/16/Z) and the National Institutes of Health (Grant Number R01EB028772). Sensor development was made possible by funding from the National Institutes of Health (R44MH110288).

CONFLICTS OF INTEREST

V.S. is the founding director of QuSpin, a commercial entity selling OPM magnetometers. J.O. and C.D. are employees of QuSpin. E.B. and M.J.B. are directors of Cerca Magnetics Limited, a spin-out company whose aim is to commercialise aspects of OPM-MEG technology. E.B., M.J.B., R.B., N.H. and R.H. hold founding equity in Cerca Magnetics Limited. HS, FW, and TH are employees of Cerca Magnetics Limited.

REFERENCES

1. Barone, J. & Rossiter, H. E. Understanding the Role of Sensorimotor Beta Oscillations. *Frontiers in Systems Neuroscience* **15**, (2021).
2. Pfurtscheller, G. & Lopes da Silva, F. H. Event-related EEG/MEG synchronization and desynchronization: Basic principles. *Clin Neurophysio* **110**, 1842–1857 (1999).
3. Ronconi, L. *et al.* Altered neural oscillations and connectivity in the beta band underlie detail-oriented visual processing in autism. *NeuroImage: Clinical* **28**, 102484 (2020).
4. Barratt, E. L. *et al.* Abnormal task driven neural oscillations in multiple sclerosis: A visuomotor MEG study. *Human Brain Mapping* **38**, 2441–2453 (2017).
5. Little, S. & Brown, P. The functional role of beta oscillations in Parkinson's disease. *Parkinsonism & Related Disorders* **20**, S44–S48 (2014).
6. Gascoyne, L. E. *et al.* Motor-related oscillatory activity in schizophrenia according to phase of illness and clinical symptom severity. *NeuroImage: Clinical* **29**, 102524 (2021).

7. Gaetz, W., Macdonald, M., Cheyne, D. & Snead, O. Neuromagnetic imaging of movement-related cortical oscillations in children and adults: Age predicts post-movement beta rebound. *Neuroimage* **51**, 792–807 (2010).
8. Kurz, M. J. *et al.* Developmental Trajectory of Beta Cortical Oscillatory Activity During a Knee Motor Task. *Brain Topogr* **29**, 824–833 (2016).
9. Trevarrow, M. P. *et al.* The developmental trajectory of sensorimotor cortical oscillations. *NeuroImage* **184**, 455–461 (2019).
10. Vakhtin, A. A., Kodituwakku, P. W., Garcia, C. M. & Tesche, C. D. Aberrant development of post-movement beta rebound in adolescents and young adults with fetal alcohol spectrum disorders. *NeuroImage: Clinical* **9**, 392–400 (2015).
11. Candelaria-Cook, F. T. *et al.* Developmental trajectory of MEG resting-state oscillatory activity in children and adolescents: a longitudinal reliability study. *Cerebral Cortex* **32**, 5404–5419 (2022).
12. Clarke, A. R., Barry, R. J., McCarthy, R. & Selikowitz, M. Age and sex effects in the EEG: development of the normal child. *Clinical Neurophysiology* **112**, 806–814 (2001).
13. Whitford, T. J. *et al.* Brain maturation in adolescence: Concurrent changes in neuroanatomy and neurophysiology. *Human Brain Mapping* **28**, 228–237 (2007).
14. Hunt, B. A. E. *et al.* Spatial and spectral trajectories in typical neurodevelopment from childhood to middle age. *Network Neuroscience* **3**, 497–520 (2019).
15. Ott, L. R. *et al.* Spontaneous cortical MEG activity undergoes unique age- and sex-related changes during the transition to adolescence. *NeuroImage* **244**, 118552 (2021).
16. Brookes, M. J. *et al.* Investigating the Electrophysiological Basis of Resting State Networks using Magnetoencephalography. *Proceedings of the National Academy of Science USA* **108**, 16783–16788 (2011).
17. Brookes, M. J. *et al.* Measuring functional connectivity using MEG: Methodology and comparison with fcMRI. *NeuroImage* **56**, 1082–1104 (2011).
18. Schäfer, C. B., Morgan, B. R., Ye, A. X., Taylor, M. J. & Doesburg, S. M. Oscillations, networks, and their development: MEG connectivity changes with age. *Human Brain Mapping* **35**, 5249–5261 (2014).

19. Brookes, M. J. *et al.* Altered temporal stability in dynamic neural networks underlies connectivity changes in neurodevelopment. *NeuroImage* **174**, 563–575 (2018).
20. Vorperian, H. K. *et al.* Estimating Head Circumference from Pediatric Imaging Studies: An Improved Method. *Academic Radiology* **14**, 1102–1107 (2007).
21. Whitham, E. M. *et al.* Scalp electrical recording during paralysis: Quantitative evidence that EEG frequencies above 20Hz are contaminated by EMG. *Clinical Neurophysiology* **118**, 1877–1888 (2007).
22. Brookes, M. J. *et al.* Magnetoencephalography with optically pumped magnetometers (OPM-MEG): the next generation of functional neuroimaging. *Trends in Neurosciences* **45**, 621–634 (2022).
23. Boto, E. *et al.* Moving magnetoencephalography towards real-world applications with a wearable system. *Nature* (2018) doi:10.1038/nature26147.
24. Hill, R. M. *et al.* A tool for functional brain imaging with lifespan compliance. *Nature Communications* **10**, 1–11 (2019).
25. Feys, O. *et al.* On-Scalp Optically Pumped Magnetometers versus Cryogenic Magnetoencephalography for Diagnostic Evaluation of Epilepsy in School-aged Children. *Radiology* **304**, 429–434 (2022).
26. Jones, S. R. When brain rhythms aren't 'rhythmic': implication for their mechanisms and meaning. *Current Opinion in Neurobiology* **40**, 72–80 (2016).
27. Sherman, M. A. *et al.* Neural mechanisms of transient neocortical beta rhythms: Converging evidence from humans, computational modeling, monkeys, and mice. *Proceedings of the National Academy of Sciences of the United States of America* **113**, E4885–E4894 (2016).
28. Shin, H., Law, R., Tsutsui, S., Moore, C. I. & Jones, S. R. The rate of transient beta frequency events predicts behavior across tasks and species. *eLife* **6**, e29086 (2017).
29. Little, S., Bonaiuto, J., Barnes, G. & Bestmann, S. Human motor cortical beta bursts relate to movement planning and response errors. *PLoS Biology* **17**, e3000479 (2019).
30. Seedat, Z. A. *et al.* The role of transient spectral 'bursts' in functional connectivity: A magnetoencephalography study. *NeuroImage* **209**, 116537 (2020).
31. Rayson, H. *et al.* Detection and analysis of cortical beta bursts in developmental EEG data. *Developmental Cognitive Neuroscience* **54**, 101069 (2022).

32. van Ede, F., Quinn, A. J., Woolrich, M. W. & Nobre, A. C. Neural Oscillations: Sustained Rhythms or Transient Burst-Events? *Trends in Neurosciences* **41**, 415–417 (2018).
33. Baker, A. P. *et al.* Fast transient networks in spontaneous human brain activity. *eLife* **2014**, 1867 (2014).
34. Vidaurre, D. *et al.* Spectrally resolved fast transient brain states in electrophysiological data. *NeuroImage* **126**, 81–95 (2016).
35. Borna, A. *et al.* A 20-channel magnetoencephalography system based on optically pumped magnetometers. *Physics in Medicine and Biology* **62**, 8909–8923 (2017).
36. Holmes, M. *et al.* A bi-planar coil system for nulling background magnetic fields in scalp mounted magnetoencephalography. *NeuroImage* **181**, 760–774 (2018).
37. O'Neill, G. C., Barratt, E. L., Hunt, B. A. E., Tewarie, P. K. & Brookes, M. J. Measuring electrophysiological connectivity by power envelope correlation: A technical review on MEG methods. *Physics in Medicine and Biology* **60**, R271–R295 (2015).
38. Boto, E. *et al.* Measuring functional connectivity with wearable MEG. *NeuroImage* **230**, 117815 (2021).
39. Rier, L. *et al.* Mild traumatic brain injury impairs the coordination of intrinsic and motor-related neural dynamics. *NeuroImage: Clinical* **32**, 102841 (2021).
40. Ogawa, S., Lee, T. M., Kay, A. R. & Tank, D. W. Brain magnetic resonance imaging with contrast dependent on blood oxygenation. *Proceedings of the National Academy of Sciences of the United States of America* **87**, 9868–9872 (1990).
41. Chance, B., Zhuang, Z., UnAh, C., Alter, C. & Lipton, L. Cognition-activated low-frequency modulation of light absorption in human brain. *Proceedings of the National Academy of Sciences of the United States of America* **90**, 3770–3774 (1993).
42. Berger, H. Über das Elektrenkephalogramm des Menschen. *Archiv für Psychiatrie und Nervenkrankheiten* **87**, 527–570 (1929).
43. Hamalainen, M. S. *et al.* Magnetoencephalography: Theory, instrumentation, and applications to non-invasive studies of the working human brain. *Reviews of Modern Physics* **65**, 413–497 (1993).
44. Allred, J., Lyman, R., Kornack, T. & Romalis, M. V. High-sensitivity atomic magnetometer unaffected by spin-exchange relaxation. *Physical Review Letters* **89**, Article Number: 130801 (2002).

45. Boto, E. *et al.* Triaxial detection of the neuromagnetic field using optically pumped magnetometry: feasibility and application in children. *NeuroImage* **252**, 119027 (2022).
46. Brookes, M. J. *et al.* Theoretical advantages of a triaxial optically pumped magnetometer magnetoencephalography system. *NeuroImage* **236**, 118025 (2021).
47. Tierney, T. M., Mellor, S., O'Neill, G. C., Timms, R. C. & Barnes, G. R. Spherical harmonic based noise rejection and neuronal sampling with multi-axis OPMs. *NeuroImage* 119338 (2022).
48. Specchio, N. *et al.* International League Against Epilepsy classification and definition of epilepsy syndromes with onset in childhood: Position paper by the ILAE Task Force on Nosology and Definitions. *Epilepsia* **63**, 1398–1442 (2022).
49. Lamberink, H. J. *et al.* Seizure outcome and use of antiepileptic drugs after epilepsy surgery according to histopathological diagnosis: a retrospective multicentre cohort study. *The Lancet Neurology* **19**, 748–757 (2020).
50. Bauer, M., Stenner, M.-P., Friston, K. J. & Dolan, R. J. Attentional Modulation of Alpha/Beta and Gamma Oscillations Reflect Functionally Distinct Processes. *Journal of Neuroscience* (2014) doi:10.1523/JNEUROSCI.3474-13.2014.
51. Tewarie, P. *et al.* Relationships Between Neuronal Oscillatory Amplitude and Dynamic Functional Connectivity. *Cerebral Cortex* **29**, 2668–2681 (2019).
52. Barratt, E. L., Francis, S. T., Morris, P. G. & Brookes, M. J. Mapping the topological organisation of beta oscillations in motor cortex using MEG. *NeuroImage* **181**, 831–844 (2018).
53. Holmes, N. *et al.* Enabling ambulatory movement in wearable magnetoencephalography with matrix coil active magnetic shielding. *NeuroImage* **274**, 120157 (2023).
54. Altarev, I. *et al.* A magnetically shielded room with ultra low residual field and gradient. *Rev Sci Instrum* **85**, 75106 (2014).
55. Rea, M. *et al.* Precision magnetic field modelling and control for wearable magnetoencephalography. *NeuroImage* **241**, 118401 (2021).
56. Rhodes, N. *et al.* Measurement of Frontal Midline Theta Oscillations using OPM-MEG. *NeuroImage* **271**, 120024 (2023).

57. Borna, A. *et al.* Cross-Axis projection error in optically pumped magnetometers and its implication for magnetoencephalography systems. *NeuroImage* **247**, 118818 (2022).

58. Richards, J. Neurodevelopmental MRI Database. (2019) doi:10.25790/BML0CM.49.

59. Jenkinson, M., Bannister, P., Brady, M. & Smith, S. Improved Optimization for the Robust and Accurate Linear Registration and Motion Correction of Brain Images. (2002) doi:10.1006/nimg.2002.1132.

60. Jenkinson, M. & Smith, S. A global optimisation method for robust affine registration of brain images. *Medical Image Analysis* **5**, 143–156 (2001).

61. Zetter, R., Iivanainen, J. & Parkkonen, L. Optical Co-registration of MRI and On-scalp MEG. *Scientific Reports 2019 9:1* **9**, 1–9 (2019).

62. Hill, R. M. *et al.* Multi-channel whole-head OPM-MEG: Helmet design and a comparison with a conventional system. *NeuroImage* **219**, 116995 (2020).

63. Rier, L. *et al.* Test-Retest Reliability of the Human Connectome: An OPM-MEG study. *Imaging Neuroscience* (2023) doi:10.1162/imag_a_00020.

64. Cignoni, P. *et al.* MeshLab: An open-source mesh processing tool. in *6th Eurographics Italian Chapter Conference 2008 - Proceedings* 129–136 (2008).

65. Oostenveld, R., Fries, P., Maris, E. & Schoffelen, J. M. FieldTrip: Open source software for advanced analysis of MEG, EEG, and invasive electrophysiological data. *Computational Intelligence and Neuroscience* **2011**, (2011).

66. Tierney, T. M. *et al.* Modelling optically pumped magnetometer interference in MEG as a spatially homogeneous magnetic field. *NeuroImage* **244**, 118484 (2021).

67. Van Veen, B. D., van Drongelen, W., Yuchtman, M. & Suzuki, A. Localization of brain electrical activity via linearly constrained minimum variance spatial filtering. *IEEE transactions on bio-medical engineering* **44**, 867–80 (1997).

68. Nolte, G. The magnetic lead field theorem in the quasi-static approximation and its use for magnetoenchephalography forward calculation in realistic volume conductors. *Physics in Medicine and Biology* **48**, 3637–3652 (2003).

69. Tzourio-Mazoyer, N. *et al.* Automated anatomical labeling of activations in SPM using a macroscopic anatomical parcellation of the MNI MRI single-subject brain. *NeuroImage* **15**, 273–289 (2002).

70. Hillebrand, A. *et al.* Direction of information flow in large-scale resting-state networks is frequency-dependent. *Proceedings of the National Academy of Sciences of the United States of America* **113**, 3867–3872 (2016).

71. Gong, G. *et al.* Age- and gender-related differences in the cortical anatomical network. *Journal of Neuroscience* **29**, 15684–15693 (2009).

72. Brookes, M. J., Woolrich, M. W. & Barnes, G. R. Measuring functional connectivity in MEG: A multivariate approach insensitive to linear source leakage. *NeuroImage* **63**, 910–920 (2012).

73. Hipp, J. F., Hawellek, D. J., Corbetta, M., Siegel, M. & Engel, A. K. Large-scale cortical correlation structure of spontaneous oscillatory activity. *Nature Neuroscience* **15**, 884–890 (2012).

THE NEURODEVELOPMENTAL TRAJECTORY OF BETA BAND OSCILLATIONS: AN OPM-MEG STUDY SUPPLEMENTARY INFORMATION

Lukas Rier[+], Natalie Rhodes[+], Daisie Pakenham, Elena Boto, Niall Holmes, Ryan M. Hill, Gonzalo Reina Rivero, Vishal Shah, Cody Doyle, James Osborne, Richard Bowtell, Margot J. Taylor and Matthew J. Brookes

+Indicates authors who made equal contributions to this manuscript.

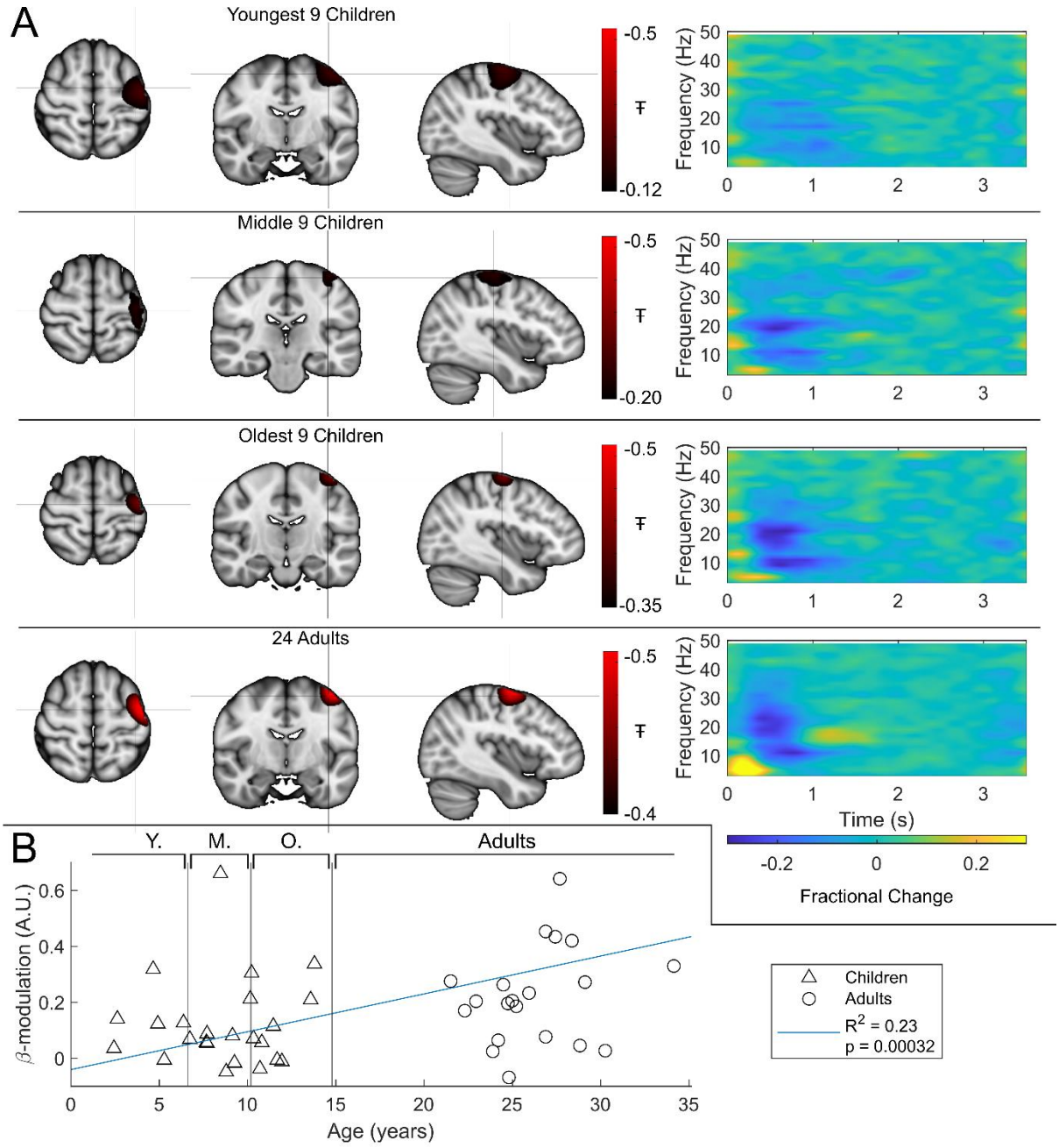

Figure S 1: Beta band modulation with age for little finger stimulation: *(A) Brain plots show slices through the left motor cortex, with a pseudo-T-statistical map of beta modulation (blue/black) overlaid on the standard brain. Time frequency spectrograms show modulation of the amplitude of neural oscillations (fractional change in spectral power relative to the baseline measured in the 2.5-3 s window). In all cases results were extracted from the location of peak beta power reduction during stimulation (in the left sensorimotor cortex). (B) Difference in beta-band amplitude (0.3-0.8 s window vs 1-1.5 s window) plotted as a function of age (i.e., each data point shows a different participant; triangles represent children, circles represent adults). Note the significant correlation (*R^2*=0.23, p=0.00032*).*

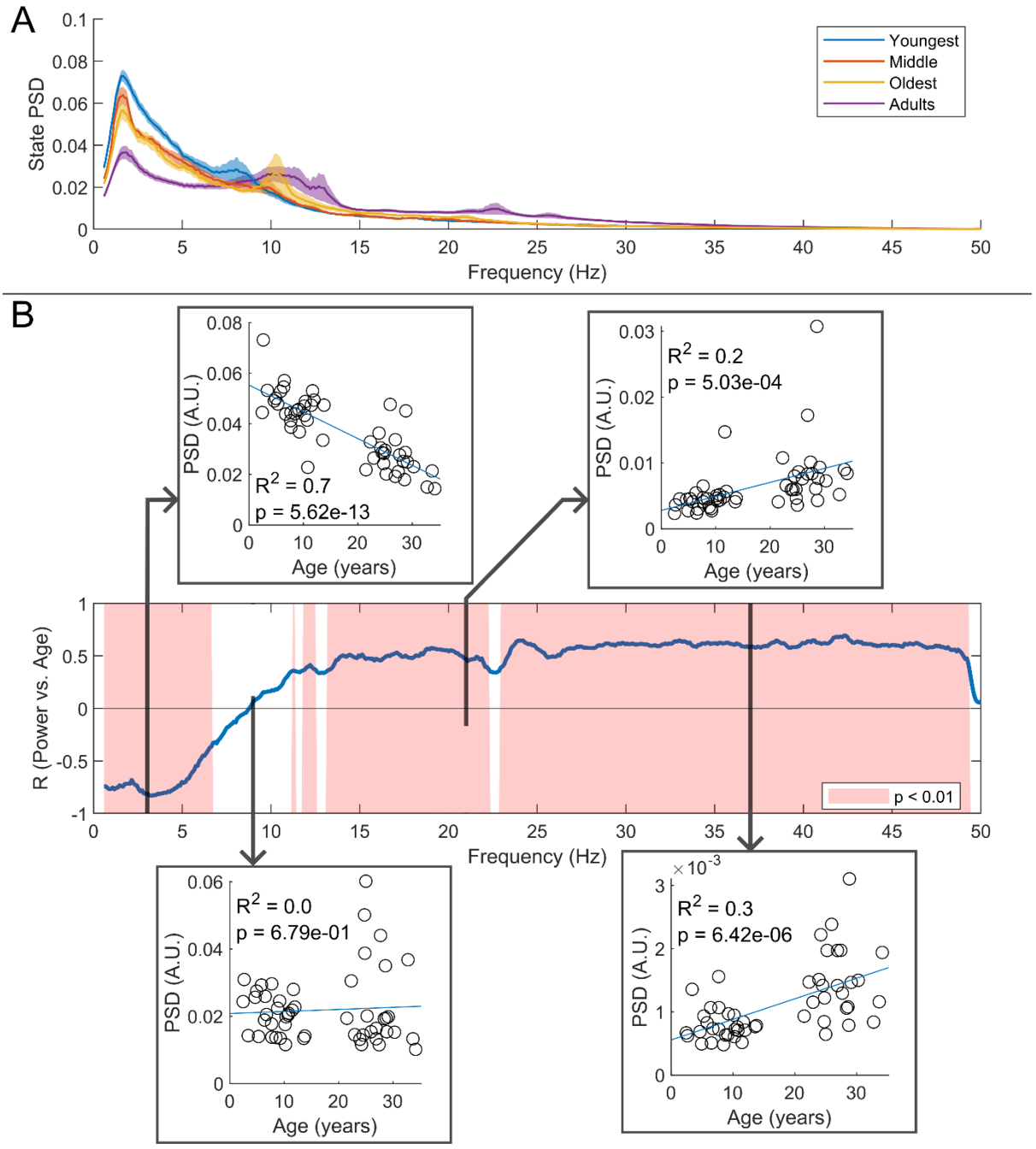

Figure S 2 Spectral content of the non-burst states*. (A) Average* ***non****-burst-state spectra across groups. Shaded areas indicate standard error on the group mean. (B) Pearson correlation coefficient for the PSD values in (A) against age across all frequency values. Red shaded areas indicate* $p < 0.01$ *(uncorrected). The four inset plots show example scatters of PSD values with age at select frequencies (3 Hz, 9 Hz, 21 Hz, and 37 Hz). Low-frequency spectral content decreases with age while high-frequency content increases. Results broadly mirror the frequency content and age relationships found in the burst state, however, features in the spectra corresponding to classical alpha and beta peaks are less prominent outside the burst state.*